


Tumor Recurrence Targeting in Active Soft Matter

Stefan Z. Stefanov¹, Irina Trifonova² 

¹ESO EAD, Sofia, Bulgaria

²Specialized Hospital for Active Treatment in Oncology, Sofia, Bulgaria

Email: stefanovsz@abv.bg, itrifa@abv.bg

How to cite this paper: Stefanov, S.Z. and Trifonova, I. (2026) Tumor Recurrence Targeting in Active Soft Matter. *Open Journal of Biophysics*, 16, 21-33.
<https://doi.org/10.4236/ojbiphy.2026.162002>

Received: March 31, 2026

Accepted: April 20, 2026

Published: April 23, 2026

Copyright © 2026 by author(s) and Scientific Research Publishing Inc.
This work is licensed under the Creative Commons Attribution International License (CC BY 4.0).

<http://creativecommons.org/licenses/by/4.0/>



Open Access

Abstract

In this paper, tumor recurrence targeting in active soft matter is developed via temperature-triggered drug release. This is done through probing and retrieving knowledge for heat in the considered soft matter, distinguishing the microenvironment from the tumor in it, and generating the energy current from the microenvironment into the tumor. Tumor targeting intensity and stability are found. Dose scheduling is set for this targeting: dose timing with three dosing moments, which are the moments of typical time and dose modulation, depending on tumor targeting intensity. This dose scheduling is valid at stable tumor targeting. Therapy schemes are simulated for 21 patients with breast cancer.

Keywords

Targeting, Active Soft Matter, Tumor Recurrence, Temperature-Triggered Drug Release

1. Introduction

The primary goal in oncology treatment is to achieve maximum survival while maintaining optimal quality of life. Advanced genetic opportunities for circulating tumor DNA (ctDNA) research have introduced the notion of minimal residual disease (MRD), which is directly correlated with predicting long-term cancer outcomes. It turns out that achieving MRD depends not so much on the size of the primary tumor as on its biological characteristics. Therefore, standard chemotherapy, which operates with maximally tolerable doses at strictly fixed intervals of administration, may not succeed in achieving its goal in heterogeneous tumors or those with primary resistance to the administered agent.

Adaptive therapy is a therapeutic approach that evolves in response to the temporal and spatial variability of the tumor microenvironment and cellular phenotype, as well as therapy-induced perturbations [1]. Adaptive therapy aims to achieve and maintain a minimal tumor volume while introducing various dosing regimens and time intervals [2]. The main idea is to prevent the proliferation of a resistant cell branch, which will prevail in the entire population.

Adaptive therapy of tumor cell populations aims to leverage competition between drug-sensitive and drug-resistant cells to improve tumor control [2] [3]. It is supposed that larger populations generate more competition and that the success of adaptive therapy can be attributed to competitive suppression [3].

Adaptive therapy success may be due to adaptation to different local environments, and not to competition [3]. Gaining a better understanding of the causes of the current success of adaptive therapy is critical to regimen design optimization and to successfully applying adaptive therapy not only to prostate cancer [3].

Cellular work [4] is altered in adapting to the tumor microenvironment. Thus, targeting the tumor microenvironment can be presented as a synergetic thermal therapy [5]. This combined therapy may offer synergistic effects that enhance treatment efficiency and overcome resistance mechanisms [5] [6].

Externally triggered drug delivery systems utilize external stimuli, such as temperature, to initiate drug release from implanted systems. These systems facilitate personalized medicine by granting patients control over the timing, dosage, and duration of drug release [7].

Adaptive therapy of tumor recurrence in active soft matter with a cilia-like observer [8] mimics the adaptive therapy of tumor cell populations. In this case, the active soft matter is presented as active colloidal chains with cilia-like and flagella-like motility, and the tumor recurrence in active soft matter is considered as run-away/quantum aging. Information recovery in that adaptive therapy is realized by two cilia-like quantum extremal islands. In addition, cancer growth and motility are obtained via the thermodynamic bound on work fluctuations of a movable piston.

In this paper, targeting the microenvironment of tumor recurrence will be mimicked as targeting the active soft matter with tumor recurrence in it from [8]. Therefore, the work changes will be considered in this soft matter targeting.

The objective of this paper is to develop therapy schemes for patients with breast cancer at tumor recurrence, targeting active soft matter via temperature-triggered drug release.

2. Probing

Let the Unruh-DeWitt particle detector probe [9] the active soft matter with a tumor recurrence in it as two separate quantum fields at hot and cold temperatures, employing double instantaneous detector-field interaction. Also, these two quantum fields are in Minkowski spacetime. These two separate quantum fields are the quantum field of the microenvironment (cold bath) and the quantum field

of the tumor recurrence (hot bath). As well, let the hot bath and the cold bath have temperatures $T_h = \Omega_c$ and $T_c = 0.01\Omega_c$, and let the detector have couplings λ_h and λ_c , $\lambda_h = \lambda_c = 3/\Omega_c$, and an effective size $R_d = 1/\Omega_c$. Let the temporal separation between the two instantaneous interactions, used to cool the detector, be $\Delta t_v = 2/\Omega_c$. Here, Ω_c is a cold value of the energy gap of the detector.

Let this detector extract work W_v from the microenvironment with $\Omega_c \approx 1$ and medium coupling $\lambda_h = \lambda_c \approx 3$, in such a way:

1) First probing: The detector probes the hot bath as it extracts work, traveling through the hot bath with a speed v_h , $v_h = v$, and traveling through the cold bath with a speed v_c , $v_c = 0$.

2) Second probing: The detector probes the cold bath as it extracts work, traveling to the hot bath with a speed v_h , $v_h = 0$, and traveling to the cold bath with a speed v_c , $v_c = v_a$.

3) Third probing: The detector probes the cold bath as it extracts work, traveling through the hot bath with a speed v_h , $v_h = 0$, and traveling through the cold bath with a speed v_c , $v_c = v$.

Here, v is the restoration speed from the primary tumor, $v = 20/t_r$, where t_r is the restoration time during cyclic chemotherapy in soft matter.

Here, v_a is the average velocity of an active colloidal chain with a cargo, corresponding to the amplitude of the stable boundary cycle of a large tumor interaction in soft matter with the environment at a tensile force protocol treatment [8].

Here, detector couplings λ_h and λ_c , $\lambda_h = \lambda_c \approx 3$, correspond to the tumor-specific heat capacity [10].

Then the work $W_v/10$ is found from the velocities v and v_a according to Fig. 4 in [9].

3. Work for Retrieving Knowledge

Let the retrieving knowledge for the active soft matter with a tumor recurrence in it mimic cortical neurodynamics at retrieving knowledge [11], as it enhances Otto-mobile efficiency [12] via the addition of a quantum Carnot cycle, working with the internal magnetic levels of a paramagnetic medium. Here, the Otto cycle mimics cancer growth and motility as the phase transition to a stretched mode of the polymer knot under tensile force [13]. That is possible because this phase transition is characterized by a strong peak in the heat capacity at the temperature $T_{tr,1} = 6$ and by a minor peak in the heat capacity at the temperature $T_{tr,2} = 1$. As well, cancer growth and motility can be found [8] by the thermodynamic bound on work fluctuations of a movable piston.

3.1. Heat Engine

Let the heat engine, retrieving knowledge for the active soft matter with a tumor recurrence in it, be with a combined Otto and quantum Carnot cycle from [12].

Then, the improvement of the Otto cycle efficiency [12] is based on running an additional thermodynamic cycle, namely the Carnot cycle, between the hottest

and coldest temperatures. In addition, the working fluid is represented by the internal degrees of freedom of the gas particles. Also, let each of the gas particles have internal states decoupled from the center of mass and capable of a separate thermodynamic cycle. The Otto cycle works with the center of mass degrees of freedom, while the Carnot cycle works with the internal magnetic levels of the medium. This combined cycle can have maximal possible efficiency [12].

The Otto cycle consists of two adiabatic and two isochoric processes, and its efficiency is determined by the span of temperatures T_1 and T_2 , $T_1 > T_2$, of the hotter adiabatic process. This efficiency does not depend on the temperatures T_4 and T_3 , $T_4 > T_3$, of the colder adiabatic process. Here, T_1 and T_3 are, correspondingly, the hottest and the coldest temperatures of the cycle.

Let this heat engine have the following temperatures:

1) Average work W_{ad} at adaptive therapy with a cilia-like observer [8] of tumor recurrence in soft active matter and the probing work W_r from §2 define the following temperature T_4 :

$$T_4 = (W_{ad} + \text{abs}(W_r)) / ((5/6)k \ln(2)), k = 0.695 \quad (1)$$

Here, k is the Boltzmann constant, and $\text{abs}()$ denotes the absolute value.

2) The Otto cycle efficiency is determined [12] by the volume span, or equivalently, by the temperature span of the hotter adiabatic process. Then [12]:

$$T_2 = T_1 (V_1/V_2)^{(\gamma-1)/\gamma} \quad (2)$$

Here, γ is the heat capacity ratio of the working fluid, which is a diatomic gas (dry air). Then $\gamma = 7/5$.

Let the adiabatic expansion of the volume from (2) be the adiabatic expansion of the volume of the cell [8] with the work-distribution parameter α , $\alpha = (V_1/V_2)^{2/d} - 1$. Then:

$$T_2 = T_{r,2} ((\alpha + 1)^{d/2})^{(\gamma-1)/\gamma}, T_{r,2} = 1 \quad (3)$$

Here, d is the dimensionality of the active soft matter with a tumor recurrence in it [8].

3) Let the temperature T_1 be defined by the temperature $T_{r,1}$, $T_{r,1} = 6$, and the temperatures T_2 and T_4 of the adiabatic process in the following way:

$$T_1 = (T_{r,1} T_2 T_4)^{1/2}, T_{r,1} = 6 \quad (4)$$

4) Temperature T_3 is found from the ratio of the temperatures of the adiabatic process:

$$T_3 = T_2 T_4 / T_1 \quad (5)$$

3.2. Combined Cycle Efficiency

At the Otto cycle, the heat given to the considered soft matter Q_0 is given by the following limiting value [12]:

$$Q_0 = (k/(\gamma - 1))(T_1 - T_4) \quad (6)$$

In the limiting case, the work produced by the above Otto cycle is [12]:

$$W_0 = (k/(\gamma-1))(T_1 - T_4)(1 - T_2/T_1) \quad (7)$$

The efficiency of this Otto cycle in the limiting case is:

$$\eta_0 = W_0/Q_0 \quad (8)$$

At the Carnot cycle, the heat given to the considered soft matter Q_c has the following limiting value [12]:

$$Q_c = kT_1 \ln(N) \quad (9)$$

In the limiting case, the work produced by the above Carnot cycle is [12]:

$$W_c = k(T_1 - T_3) \ln(N) \quad (10)$$

The efficiency of this Otto cycle in the limiting case is:

$$\eta_c = W_c/Q_c \quad (11)$$

In (6), (7), (9), and (10), k is the Boltzmann constant, γ is the heat capacity ratio of the working fluid, $\ln(\cdot)$ is the natural logarithm, and N is the number of microstates of the active soft matter at adaptive therapy with a cilia-like observer [8].

The efficiency of the combined Otto and Carnot cycle in the limiting case is:

$$\eta = (W_0 + W_c)/(Q_0 + Q_c) \quad (12)$$

The efficiency (12) is the maximum possible efficiency of the considered combined Otto and Carnot cycles [12].

3.3. Tumor Interaction with the Microenvironment

Let the tumor microenvironment be a cold bath for the tumor. Let this cold bath be a periodic one-dimensional XX spin chain with spins $\frac{1}{2}$ on the sites. Let the above heat engine be a single site, interacting with the cold bath only through the first site.

The trade-off between efficiency and speed in quantum heat engines allows [14] the finding of the microenvironment heat capacity as the renormalized quantum Fisher information of the cold bath. Indeed, in [14], the renormalized Fisher information of the cold bath corresponds to the heat capacity of the cold bath per unit volume. Then the microenvironment heat capacity c_h is:

$$c_h = (1/N)(2/\Delta t)^{d/2} Q_c^2 / \left(8\beta(Q_0 + Q_c)(2\pi\nu)^{d/2} (\eta - \eta_0) \right) \quad (13)$$

where β is the inverse temperature, $\beta \approx 1$, d is the spatial dimension, and Δt is the time-like width of information recovery at the adaptive therapy with a cilia-like observer [8].

Tumor interaction with the considered microenvironment is determined by the interaction constant of this spin chain. Then [14] this interaction J_0 can be found from the following equation:

$$(1/N)8\beta J_0^3 / \left(1 + \exp(-\beta J_0) \right)^2 - c_h = 0 \quad (14)$$

4. Energy Current Generator

4.1. Heat Rectifier

Let the tumor have three states according to heat capacity: 1) ground state; 2) quasi-degenerate excited state, corresponding to the strong peak in the heat capacity at temperature $T_{tr,1} = 6$ from §3; 3) quasi-degenerate excited state, corresponding to the minor peak in the heat capacity at temperature $T_{tr,2} = 1$ from §3. This is the V-model [15] of the tumor heat capacity, where the tumor is a thermally conducting element, mediating stationary quantum heat transport between hot and cold thermal baths of the microenvironment.

Energy is exchanged between the baths through two parallel pathways with an imbalance between them, courtesy of a coherence parameter. Let this V-model of the tumor heat capacity be with a coherence parameter α_c , defined by the work-distribution parameter α of the adaptive therapy with a cilia-like observer (§3.1), $\alpha_c = \alpha - 1$.

Heat is absorbed by the tumor in the transition from the ground state according to the heat capacity in the quasi-degenerate excited state, corresponding to the strong peak in the heat capacity at temperature $T_{tr,1} = 6$. Heat tunnels coherently to the quasi-degenerate excited state, corresponding to the minor peak in the heat capacity at temperature $T_{tr,2} = 1$, and decays from the tumor to the cold bath.

When absorbing the heat from the tumor, the heat current j_p is found from the temperature difference ΔT_p , $\Delta T_p = T_2 - T_3$, $T_2 > T_3$, and the coherence parameter α_c from the graphic in Fig. 9(b2) in [15].

At the decays of the tumor heat, the heat current j_n is obtained from the temperature difference ΔT_n , $\Delta T_n = T_4 - T_1$, $T_1 > T_4$, and the coherence parameter α_c , according to Fig. 9(b2) in [15].

At thermal rectification, the magnitude of the heat current between the baths is different when exchanging the direction of the applied temperature bias.

4.2. Thermalization Path

Let the microenvironment be distinguished from the tumor within it, as the thermalization paths of the cosmic qubit are distinguished, undergoing non-Markovian de Sitter evolution from [16]. Let this distinguishability be through the asymptotic quantum Fisher information F_ϕ , equal to the heat current from § 4.1, for Hubble parameter H , $H = \pi/5$, when the cosmic qubit is determined by the unit energy gap and its initial state preparation. In addition, let the cosmic qubit have an initial state preparation, defined by run-away/quantum aging active soft matter at the adaptive therapy with a cilia-like observer [8].

Typical time moments, where the microenvironment differs from the tumor, are found for the above quantum Fisher information according to the graphics from Fig. 8 in [16].

Considered thermalization is with a unique end, irrelevant to the initial state preparation [16]. Therefore, the above distinction between the microenvironment and the tumor is at the final time moment. Let t_f be the final time moment, defined

for $F_q = j_n$.

Quantum Fisher information curves, at the considered thermalization, may have a single peak [16]. Then, there may be two more time moments t_1 and t_2 , before the moment t_3 , when the microenvironment is distinguished from the tumor. Let these two time moments be defined for $F_q = j_n$. If there are no such two time moments, let them be defined for $F_q = j_p$.

Distinguishing the microenvironment from the tumor is completely assigned at these three typical time moments.

4.3. Energy Current Profile

Let the tumor be a quantum spin chain with periodic boundary conditions, surrounded by non-Markovian microenvironment cold baths. Besides, let this quantum spin chain be a one-dimensional XY spin chain with Dzyaloshinskii-Moriya interaction and an external magnetic field. As well, let each spin be immersed in its own non-Markovian cold bath and the microenvironment have the same parameters for all baths.

Let this spin chain be with four sites, z -component of Dzyaloshinskii-Moriya interaction D_z , $D_z = 0.3$, uniform magnetic field B_z along the z direction, $B_z = J_0$, overall microenvironment-caused noise to the spin chain Γ , $\Gamma = 0.005$, and the memory time of the microenvironment $1/\gamma_c$, $\gamma_c = 2$. Here J_0 is the interaction from (14).

Also, let the temperature difference between the tumor and the microenvironment be $\Delta T_{sb} = 60^\circ\text{C}$. This is fulfilled for temperatures that are five or six times higher than the temperatures of the heat machine from §3.1.

Generated energy current [17] by the microenvironment to the tumor is defined for the three typical time moments t_1 , t_2 , and t_3 from Fig. 5(b) in [17]. Let the corresponding values of this current be $j_{e,1}$, $j_{e,2}$, and $j_{e,3}$.

5. Tumor Targeting

5.1. Tumor Targeting Intensity

Tumor targeting intensity $k_{h,i}$ depends on the squared released drug energy current:

$$k_{h,i} = R_d \left(10 j_{e,i} \right)^2, i = 1, 2, 3, \quad R_d = \rho \text{ if } \rho \leq 1, R_d = 1/\rho \text{ if } \rho > 1 \quad (15)$$

In (15) $j_{e,i}$ is the energy current from §4.3.

In (15) it is assumed that the released drug R_d is defined from the rectification ratio of the thermal rectification ρ [15]. The rectification ratio ρ is found from the temperature difference and the coherence parameter from §4.1, according to the graphic in Fig. 9(b2) in [15].

5.2. Tumor Targeting Stability

Tumor targeting stability depends on quantum coherence dynamics between the tumor and the microenvironment, and on the thermal rectification coherence. Therefore, a marker for tumor targeting stability $m_{s,i}$ is defined by the following

frequency $f_{u,i}$ [Hz]:

$$f_{u,i} = (2.4941c_{s,i} + c_r)10^3, i = 1, 2, 3 \quad (16)$$

In this case, if $f_{u,i} < 124.7$, then $f_{u,i} = 4f_{u,b}$ and if $f_{u,i} < 249.41$, then $f_{u,i} = 2f_{u,i}$.

In (16) $c_{s,i}$ is the quantum coherence between the tumor and the microenvironment. It is defined for three time moments t_1 , t_2 , and t_3 from Fig. 5 (b) (inset) in [17].

In (16) c_r is the quantum coherence at thermal rectification from §4.1. It is defined by the temperature difference and the coherence parameter from §4.1, according to the graphic from Fig. 9(a) in [15].

Values of this marker are found from the interval diagram of beneficial and detrimental frequency patterns in cancer [18] according to Fig. 3 in [18]. These values are:

- 1) positive, when the frequency $f_{u,i}$ is a frequency beneficial for life;
- 2) negative, when the frequency $f_{u,i}$ is a frequency detrimental to life;
- 3) Undefined when the frequency $f_{u,i}$ is outside the intervals of the beneficial and detrimental frequencies.

6. Boosted Targeting of the Microenvironment

Let the boosted targeting be realized by quantum energy teleportation via the traversable wormhole protocol from [19]. Therefore, let the heat engine from §3, entangled with the discriminator of thermalization paths from §4, extract energy. Here, the heat engine is a site from the spin chain in §3.3, and the thermalization paths discriminator is the cosmic qubit in §4.2. Let this extracted energy be [19]:

$$E_p = 0.4(2\pi/\beta)^{2/d+1} \tanh(\pi\Delta t/\beta) / \cosh(\pi\Delta t/\beta)^{2/d} \quad (17)$$

Here, β is the inverse temperature, d is the dimensionality of active soft matter with a tumor recurrence in it from §3.1, and Δt is the time-like width of information recovery at adaptive therapy with a cilia-like observer from §3.3. Also, $\tanh()$ and $\cosh()$ are the hyperbolic tangent and hyperbolic cosine, respectively.

Boosting the microenvironment targeting is achieved through relativistic quantum metrology of the temperature in $(3 + 1)$ -dimensional de Sitter space [20]. This is realized via Fisher information as a probe of spacetime structure.

Boosting the microenvironment targeting is achieved through a new capacity ratio of the working fluid. Therefore, T_n from Fig.3 in [20] is sought for asymptotic Fisher information F_s , $F_s = c_h/11.5$, and energy gap E_p . Here, c_h is the microenvironment heat capacity from (13). If such a temperature T_n can be found, then the new capacity ratio of the working fluid γ_n is defined as follows:

$$\gamma_n = 1 / (1 - (2\beta/d) \ln(T_2) / \ln(T_n + 1)) \quad (18)$$

If it is not possible to find such a temperature T_n , then $\gamma_n = 7/5$, as in §3.1.

Here, β and d are defined in (17), $\ln()$ is the natural logarithm, and T_2 is the temperature from (2).

7. Dose Scheme for Tumor Targeting

7.1. Targeting Cancer Stem Cells

Minimally invasive and broad-spectrum treatment of cancer stem cells is sought for at nanoparticle-mediated ablation therapies that can kill the cancer stem cells by utilizing heat or freezing. One of the major challenges in clinical translation of these therapies is how to specifically target cancer stem cells [21]. Therefore, it may be assumed that the tumor recurrence targeting in active matter mimics specifically targeting of cancer stem cells.

HCPN-CG nanoparticles [22] are cold-responsive nanoparticles for the targeted co-delivery of chemotherapeutics and a photothermal agent into orthotopic human mammary tumors. These cold-responsive nanoparticles can take advantage of the cold-responsive property to achieve efficient burst release of chemotherapeutics and photothermal agent upon ice cooling. Moreover, the generated localized heat under near-infrared laser irradiation can further enhance the cytotoxicity of chemotherapeutics and inhibit the growth of tumors. *In vitro* studies with both 2D-cultured cancer cells and 3D microscale tumors enriched with cancer stem cells and *in vivo* studies using orthotopic triple-negative human breast tumors grown in mice demonstrate that the HCPN-CG nanoparticles with ice cooling (5 min) followed by laser irradiation (1 W/cm², 2 min) augment cancer destruction with no evident systemic toxicity [22].

Let the dosing scheme, at tumor targeting, mimic this temperature-triggered drug release.

7.2. Dose Timing

The first dose at tumor recurrence in active soft matter is given at the $(t_1/2 + 2.5)$ -th hour, the second dose at the $(t_2/2 + 2.5)$ -th hour, and the third dose at the $(t_3/2 + 2.5)$ -th hour. Here, the typical timing from §4.2 is considered as dose timing in hours.

7.3. Dose Modulation

The value of the first dose is the tumor targeting intensity $k_{h,1}$ [μg/ml] from (15). This dose is a result of drug release, similar to localized photothermal warming-enabled chemotherapeutic drug release ((+L)-release) [22], or of drug release, similar to localized cold-triggered chemotherapeutic drug release ((+I)-release) [22]. Generated energy current from the microenvironment to the tumor is $j_{e,1}$ from §4.3.

The value of the second dose is the tumor targeting intensity $k_{h,2}$ [μg/ml] from (15). This dose is a result of drug release, similar to (+L)-release, or of the drug release, similar to (+I)-release. The generated energy current from the microenvironment to the tumor is $j_{e,2}$ from §4.3.

The value of the third dose is the tumor targeting intensity $k_{h,3}$ [μg/ml] from (15). This dose is a result of drug release, similar to (+L)-release. The generated energy current from the microenvironment to the tumor is $j_{e,3}$ from §4.3.

7.4. Scheme Characteristics

Let the dose scheme at tumor targeting be valid when the stability of the tumor targeting (§5.2) is positive at typical time moments t_2 , and t_3 .

Dose scheme, at targeting, mimics enhancing the cytotoxicity of chemotherapeutic drugs and inhibiting the net growth of the tumor at combined release, which is (+I)-release, followed by (+L)-release ((+I + L)-release) [22]. In addition, let the dose of the combined release have a value equal to the average intensity of the tumor targeting at (+I)-release and (+L)-release.

As well, the dose scheme at targeting mimics localized laser irradiation, when each of the three doses is (+L)-release.

Dose schemes at such a targeting are the following three types:

- 1) ((+I) (+I + L)): combined release, preceded by (+I) release;
- 2) ((+I + L) (+L)): combined release, followed by (+L) release;
- 3) ((+L) (+L) (+L)): three subsequent (+L) releases.

At the same time, the temperatures of the heat machine from §3.1 mimic the temperatures of the human body when they are multiplied by six at run-away tumor recurrence in active soft matter and are multiplied by five at quantum aging tumor recurrence in soft active matter. Let the scaled temperatures of the heat machine from §3.1 be $(T_{s,1}, T_{s,2}, T_{s,3}, T_{s,4})$ [°C].

8. Simulated Therapy Schemes

The database is used for 424 patients with breast cancer who were under treatment at the Clinic of Chemotherapy, Specialized Hospital for Active Treatment in Oncology, Sofia, Bulgaria, throughout 2003-2014. From this database is selected a group of 40 patients for the proliferation index PCNA investigation. It is used archival histological material-paraffin blocks. Suitable for research were 32 patients.

From these group of 32 patients five were dropped out, for whom the survival probability at cyclic chemotherapy in soft matter is indeterminate. For five more patients retrieve knowledge cannot be found for the heat with combined Otto and quantum Carnot cycle.

Therapy schemes for 21 patients with breast cancer are simulated at base recurrence tumor targeting in active soft matter through temperature-triggered drug release, as well the therapy schemes for 20 patients with breast cancer at boosted targeting. That is so, because one patient is only exposed to base targeting, according to simulation. Also, the simulation does not find a therapy scheme for one patient either at base targeting or at boosted targeting.

It is assumed that the treatment with HCPN-CG nanoparticles for these patients would have the cancer cell viability from Fig. 5 in [22]. Also, the cancer cell viability (CV) of the three scheme types is obtained in the following way:

- 1) $CV ((+I)(+I + L)) = CV (+I) CV (+I + L)$;
- 2) $CV ((+I + L) (+L)) = CV (+I + L) CV (+L)$;
- 3) $CV ((+L) (+L) (+L)) = CV (+L) CV (+L) CV (+L)$.

At the simulation is performed Akima interpolation of the graphics from [9]

and [22] and two-dimensional quasi-Hermite interpolation of the graphics from [15]-[17], and [20].

The simulation shows that:

1) The mean scaled temperatures ($T_{s,1}$, $T_{s,2}$, $T_{s,3}$, $T_{s,4}$) [$^{\circ}\text{C}$] are:

- At run-away tumor recurrence in soft active matter: a) first probing (41.3 ± 8.5 , 11.8 ± 2.2 , 6.9 ± 0.2 , 24.4 ± 4.0) [$^{\circ}\text{C}$]; b) second probing (40.9 ± 13.6 , 11.6 ± 2.6 , 6.8 ± 0.4 , 24.3 ± 10.7) [$^{\circ}\text{C}$]; c) third probing (40.3 ± 22.2 , 11.4 ± 2.8 , 6.7 ± 0.6 , 23.8 ± 12.0) [$^{\circ}\text{C}$].

- At quantum aging tumor recurrence in soft active matter: a) first probing (39.9 ± 9.7 , 9.9 ± 2.4 , 6.7 ± 0.3 , 27.0 ± 2.4) [$^{\circ}\text{C}$]; b) second probing (40.1 ± 21.2 , 9.8 ± 2.4 , 6.7 ± 0.6 , 27.6 ± 23.9) [$^{\circ}\text{C}$]; c) third probing (40.4 ± 13.3 , 10.1 ± 2.6 , 6.7 ± 0.4 , 27.2 ± 7.8) [$^{\circ}\text{C}$].

2) The mean dose timing is:

- At base targeting: a) first probing (3.4 ± 1.9) [hour]; b) second probing (5.2 ± 2.2) [hour]; c) third probing (7.1 ± 1.6) [hour].

- At boosted targeting: a) first probing (2.6 ± 0.8) [hour]; b) second probing (4.5 ± 2.1) [hour]; c) third probing (6.6 ± 2.2) [hour].

3) The mean dose modulation is:

- At base targeting: a) first probing (40.4 ± 38.4) [$\mu\text{g/ml}$]; b) second probing (40.2 ± 20.0) [$\mu\text{g/ml}$]; c) third probing (36.2 ± 11.1) [$\mu\text{g/ml}$].

- At boosted targeting: a) first probing (40.0 ± 37.8) [$\mu\text{g/ml}$]; b) second probing (42.7 ± 21.1) [$\mu\text{g/ml}$]; c) third probing (38.8 ± 11.9) [$\mu\text{g/ml}$].

4) The mean 2D cancer cell viability is:

- At base targeting: a) less than 1% for 11 patients; b) (6.0 ± 2.0) [%] for 10 patients.

- At boosted targeting: a) less than 1% for 6 patients; b) (23.0 ± 7.5) [%] for 14 patients.

5) Mean 3D microscale cancer cell viability is:

- At base targeting: a) less than 1% for 11 patients; b) (6.7 ± 4.2) [%] for 10 patients.

- At boosted targeting: a) less than 1% for 6 patients; b) (23.7 ± 8.3) [%] for 14 patients.

Comparing the simulated schemes at base targeting with those at boosted targeting shows that:

1) Boosted targeting confirms the base targeting and improves problematic cases.

2) The number of combined schemes at boosted targeting is less than that at the base targeting. This is due to the new capacity ratio of the working fluid from §6, caused by energy teleportation at boosted targeting.

9. Conclusions

In this paper, the tumor recurrence targeting in active soft matter is built by temperature-triggered drug release in the following way:

1) Three probings of the active soft matter with a tumor recurrence in it with

the Unruh-DeWitt particle detector;

2) Retrieving knowledge about the heat in the considered soft matter with the combined Otto and quantum Carnot cycle;

3) Distinguishing the microenvironment from the tumor within it at three typical moments through the heat current of the heat rectifier;

4) Generating the energy current from the microenvironment into the tumor, while there is an interaction between them, defined by the trade-off between efficiency and speed in the above quantum heat engine;

5) Tumor targeting intensity, found as the released drug from the energy current;

6) Tumor targeting stability, obtained by the quantum coherence between the tumor and the microenvironment, and from the thermal rectification coherence;

7) Boosted targeting of the considered soft matter, achieved by quantum energy teleportation;

8) Dose scheduling of tumor targeting: a) dose timing with dose moments, defined as the moments of the typical time; b) dose modulation, defined by the tumor-targeting intensity;

9) Dose scheduling characterization, at targeting, as it is valid at stable tumor targeting;

10) Simulation of therapy schemes targeting 21 patients with breast cancer, when the therapy targeting is similar to the therapy with HCPN-CG nanoparticles.

Conflicts of Interest

The authors declare no conflicts of interest regarding the publication of this paper.

References

- [1] Gatenby, R.A., Silva, A.S., Gillies, R.J. and Frieden, B.R. (2009) Adaptive Therapy. *Cancer Research*, **69**, 4894-4903. <https://doi.org/10.1158/0008-5472.can-08-3658>
- [2] West, J., Adler, F., Gallaher, J., Strobl, M., Brady-Nicholls, R., Brown, J., *et al.* (2023) A Survey of Open Questions in Adaptive Therapy: Bridging Mathematics and Clinical Translation. *eLife*, **12**, e84263. <https://doi.org/10.7554/elife.84263>
- [3] Hansen, E. and Read, A.F. (2020) Modifying Adaptive Therapy to Enhance Competitive Suppression. *Cancers*, **12**, Article No. 3556. <https://doi.org/10.3390/cancers12123556>
- [4] Hanselmann, R.G. and Welter, C. (2022) Origin of Cancer: Cell Work Is the Key to Understanding Cancer Initiation and Progression. *Frontiers in Cell and Developmental Biology*, **10**, Article 787995. <https://doi.org/10.3389/fcell.2022.787995>
- [5] Dai, Q., Cao, B., Zhao, S. and Zhang, A. (2022) Synergetic Thermal Therapy for Cancer: State-of-the-Art and the Future. *Bioengineering*, **9**, Article 474. <https://doi.org/10.3390/bioengineering9090474>
- [6] El-Tanani, M., Rabbani, S.A., Babiker, R., Rangraze, I., Kapre, S., Palakurthi, S.S., *et al.* (2024) Unraveling the Tumor Microenvironment: Insights into Cancer Metastasis and Therapeutic Strategies. *Cancer Letters*, **591**, Article 216894. <https://doi.org/10.1016/j.canlet.2024.216894>

- [7] Hu, H., Busa, P., Zhao, Y. and Zhao, C. (2024) Externally Triggered Drug Delivery Systems. *Smart Materials in Medicine*, **5**, 386-408. <https://doi.org/10.1016/j.smain.2024.08.004>
- [8] Stefanov, S.Z. and Trifonova, I. (2024) Cilia-Like Observer for Tumor Recurrence in Active Soft Matter. *Biophysical Reviews and Letters*, **19**, 17-35. <https://doi.org/10.1142/s1793048024500024>
- [9] Kollas, N.K. and Moustos, D. (2024) An Exactly Solvable Relativistic Quantum Otto Engine. *Physical Review D*, **109**, Article 065025. <https://doi.org/10.1103/physrevd.109.065025>
- [10] Vaupel, P. and Piazena, H. (2022) Strong Correlation between Specific Heat Capacity and Water Content in Human Tissues Suggests Preferred Heat Deposition in Malignant Tumors Upon Electromagnetic Irradiation. *International Journal of Hyperthermia*, **39**, 987-997. <https://doi.org/10.1080/02656736.2022.2067596>
- [11] Capolupo, A., Freeman, W.J. and Vitiello, G. (2013) Dissipation of 'Dark Energy' by Cortex in Knowledge Retrieval. *Physics of Life Reviews*, **10**, 85-94. <https://doi.org/10.1016/j.plrev.2013.01.001>
- [12] Opatrný, T. and Scully, M.O. (2002) Enhancing Otto-Mobile Efficiency via Addition of a Quantum Carnot Cycle. *Fortschritte der Physik*, **50**, 657-663.
- [13] Zhao, Y. and Ferrari, F. (2017) Topological Effects on the Mechanical Properties of Polymer Knots. *Physica A: Statistical Mechanics and Its Applications*, **486**, 44-64. <https://doi.org/10.1016/j.physa.2017.05.015>
- [14] Shiraishi, N. and Tajima, H. (2017) Efficiency versus Speed in Quantum Heat Engines: Rigorous Constraint from Lieb-Robinson Bound. *Physical Review E*, **96**, Article 022138. <https://doi.org/10.1103/physreve.96.022138>
- [15] Ivander, F., Anto-Sztrikacs, N. and Segal, D. (2022) Quantum Coherence-Control of Thermal Energy Transport: The V Model as a Case Study. *New Journal of Physics*, **24**, Article 103010. <https://doi.org/10.1088/1367-2630/ac9498>
- [16] Chen, L. and Feng, J. (2025) Quantum Fisher Information of a Cosmic Qubit Undergoing Non-Markovian De Sitter Evolution. *Journal of High Energy Physics*, **2025**, Article No. 29. [https://doi.org/10.1007/jhep06\(2025\)029](https://doi.org/10.1007/jhep06(2025)029)
- [17] Ablimit, A., He, R.H., Xie, Y.Y., Wu, L.A. and Wang, Z.M. (2022) Quantum Energy Current Induced Coherence in a Spin Chain under Non-Markovian Environments. *Entropy*, **24**, Article 1406. <https://doi.org/10.3390/e24101406>
- [18] Meijer, D.K.F. and Geesink, H.J.H. (2018) Favourable and Unfavourable EMF Frequency Patterns in Cancer: Perspectives for Improved Therapy and Prevention. *Journal of Cancer Therapy*, **9**, 188-230. <https://doi.org/10.4236/jct.2018.93019>
- [19] Wang, J. and Yao, S. (2024) Quantum Energy Teleportation versus Information Teleportation. *Quantum*, **8**, Article 1564. <https://doi.org/10.22331/q-2024-12-12-1564>
- [20] Du, H. and Mann, R.B. (2021) Fisher Information as a Probe of Spacetime Structure: Relativistic Quantum Metrology in (A)dS. *Journal of High Energy Physics*, **2021**, Article No. 112. [https://doi.org/10.1007/jhep05\(2021\)112](https://doi.org/10.1007/jhep05(2021)112)
- [21] Pan, Y., Liu, L., Rao, L. and Chen, X. (2022) Nanomaterial-Mediated Ablation Therapy for Cancer Stem Cells. *Matter*, **5**, 1367-1390. <https://doi.org/10.1016/j.matt.2022.02.015>
- [22] Wang, H., Agarwal, P., Liang, Y., Xu, J., Zhao, G., Tkaczuk, K.H.R., *et al.* (2018) Enhanced Cancer Therapy with Cold-Controlled Drug Release and Photothermal Warming Enabled by One Nanoplatform. *Biomaterials*, **180**, 265-278. <https://doi.org/10.1016/j.biomaterials.2018.07.021>